Rock Mechanics and Rock Engineering (2022) 55:7307–7330
https://doi.org/10.1007/s00603-022-02996-4

TECHNICAL NOTE

Stability of Unlined Elliptical Tunnels in Rock Masses

Jim Shiau[1] · Suraparb Keawsawasvong[2] · Sorawit Seehavong[2]

Received: 14 July 2021 / Accepted: 4 July 2022 / Published online: 31 July 2022

Highlights

- A state of art approach to evaluate the elliptical tunnel stability of Hoek–Brown rock mass.
- Rigorous upper bound and lower bound solutions of elliptical tunnel stability are derived using advanced finite element limit analysis.
- Comprehensive design tables and equations are proposed for stability evaluation.

Keywords Elliptical tunnels · Rock mass · Hoek–Brown · Finite element limit analysis · Design equation

1 Introduction

The application of elliptical or quasi-rectangular tunnel sections has received much attention in recent years due to the need to reduce the volume of soils excavated as well as to better utilize tunnel space. The spaces at the top and the bottom of circular tunnels are indeed unneeded as the trains are straight-edged in shape. Elliptical (oval-shaped) tunnels are, therefore, preferred, and a new "composite circular" shield tunneling machine was first developed with an adjustable cutter to bore the elliptical tunnel in the Fukutoshin Line, a new subway line in Tokyo in 2008 (Akagi 2004).

In recent years, a new quasi-rectangular earth pressure balance (EPB) shield machine has recently been developed for Ningbo railway transit in China (Liu et al. 2021). The machine consists of 4 arcs and the lining ring is divided into 11 pieces. As stated by Liu et al. (2021), the filling and diffusion process of synchronous grouting in the shield tail void is significantly different from a circular shield and the quality of the tail grouting has a dominant effect on the overall stability during the construction. Indeed, when comparing with other standard tunnel sections, elliptical tunnels are more challenging to construct and the stability evaluation is of paramount importance to ensure the safety of such a unique tunnel shape (Amberg 1983; Hochmuth et al. 1987; Wone et al. 2003; Miura 2003; Miura et al. 2003).

Very few studies were reported in relation to the stability study of elliptical tunnels. Only recently in soil stability, Yang et al. (2015, 2016) studied the stability of unlined elliptical tunnel using the numerical upper bound method. An extended work of the stability solutions of elliptical tunnels considering internal normal stress along the tunnel periphery was later presented by Zhang et al. (2017) and Bhattacharya and Dutta (2021) for cohesionless and cohesive-frictional soils. For elliptical tunnel excavations in rock masses, to the best of our knowledge, there is none. To fill the research gap, this paper proposes a stability study for elliptical tunnel stability in rock mass using advanced upper and lower bound analyses using finite elements and nonlinear programming techniques.

For rock stability study, the Hoek–Brown (HB) model (Hoek and Brown 1980; Hoek et al. 2002) is a well-recognized failure criterion that includes the nonlinearity of the minor principal (compressive) stress. The formula of the HB failure criterion is in the form of a power-law relationship between the major and minor principal stresses (i.e., σ_1 and σ_3). Taking tensile normal stresses as positive, Eq. (1) describes the HB failure criteria in a mathematical form:

$$\sigma_3 = \sigma_1 - \left(-m_b\sigma_1(-\sigma_{ci})^{(1-a)/a} + s(-\sigma_{ci})^{1/a}\right)^a, \quad (1)$$

where σ_{ci} is the uniaxial compressive strength of intact rock mass and the parameters m_b, s, and a are expressed in Eqs. (2)–(4):

✉ Suraparb Keawsawasvong
ksurapar@engr.tu.ac.th

[1] School of Engineering, University of Southern Queensland, Toowoomba, QLD 4350, Australia

[2] Department of Civil Engineering, Thammasat School of Engineering, Thammasat University, Pathumthani 12120, Thailand

$$a = \frac{1}{2} + \frac{1}{6}\left\{\exp\left(\frac{-\mathrm{GSI}}{15}\right) - \exp\left(\frac{-20}{3}\right)\right\}, \quad (2)$$

$$m_b = m_i \exp\left(\frac{\mathrm{GSI} - 100}{28 - 14\mathrm{DF}}\right), \quad (3)$$

$$s = \exp\left(\frac{\mathrm{GSI} - 100}{9 - 3\mathrm{DF}}\right). \quad (4)$$

In Eqs. (2)–(4), the geological strength index (GSI) has typical values from 10 to 100 (extremely poor rock mass to a perfectly intact rock mass). DF represents the degree of disturbance and it has typical values from 0 (undisturbed in-situ rock masses) to 1 (extremely disturbing in-situ rock masses). The parameter m_i a material constant that is related to the frictional strength of an intact rock mass and has typical values from 5 to 30. Noting that these empirical parameters have been widely adopted by the rock mechanics community, in spite that geological observations are not always in line with the semi-empirical criterion.

Several researchers have recently studied the stability of tunnels in rock masses obeying the HB failure criterion. The rock stability of unlined circular was investigated by Zhang et al. (2019) and Keawsawasvong and Ukritchon (2020), while unlined square and rectangular tunnels in rock mass were studied by Xiao et al. (2019, 2021) and Ukritchon and Keawsawasvong (2019a). Further, the rock stability of plane strain heading of tunnels was investigated by Ukritchon and Keawsawasvong (2019b). As stated before, the stability solutions of unlined elliptical tunnels in HB rock mass have never been presented in the literature. It is, therefore, the aim of this paper to produce useful stability charts and equations for geotechnical practitioners to estimate the stability of shallow unlined elliptical tunnels in rock masses obeying the Hoek–Brown failure criterion.

2 Problem Scope and Numerical Modelling

2.1 Statement of the Problem

Figure 1 shows the problem definition of an unlined elliptical tunnel in a rock mass. The tunnel has a cover depth of C. The shape of the tunnel is an ellipse with a horizontal dimension of B and a vertical dimension of D. The standard equation of an ellipse with center (0,0) and major axis parallel to the x-axis is presented in the following equation:

$$\frac{x^2}{a^2} + \frac{y^2}{b^2} = 1, \quad (5)$$

where $B = 2a$ and $D = 2b$. Equation (5) was used to generate the tunnel geometry throughout the parametric study in the paper. Figure 2a–c presents three typical model geometry so generated for a depth ratio $C/D = 2$ and different values of $B/D = 0.5$, 1, 2, respectively. The rock mass has a unit weight of γ, and at the surface area of rock masses, a uniform surcharge pressure σ_s is applied over the area.

It is hypothesized that no disturbance in the surrounding rock mass during tunnel excavation and the undisturbed

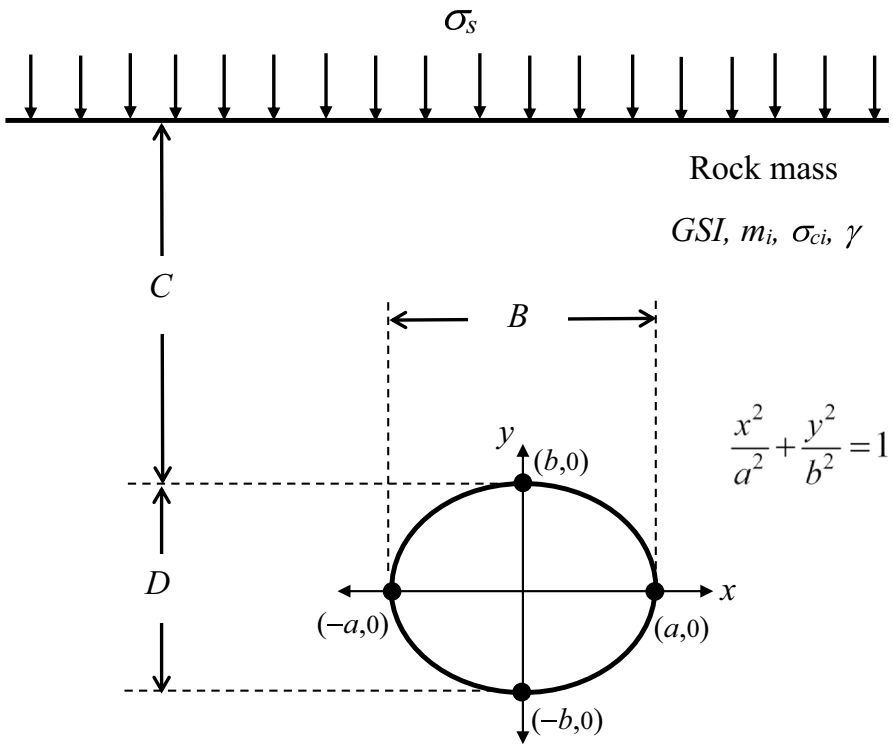

Fig. 1 Problem definition of an unsupported infinitely long elliptical tunnel in a rock mass

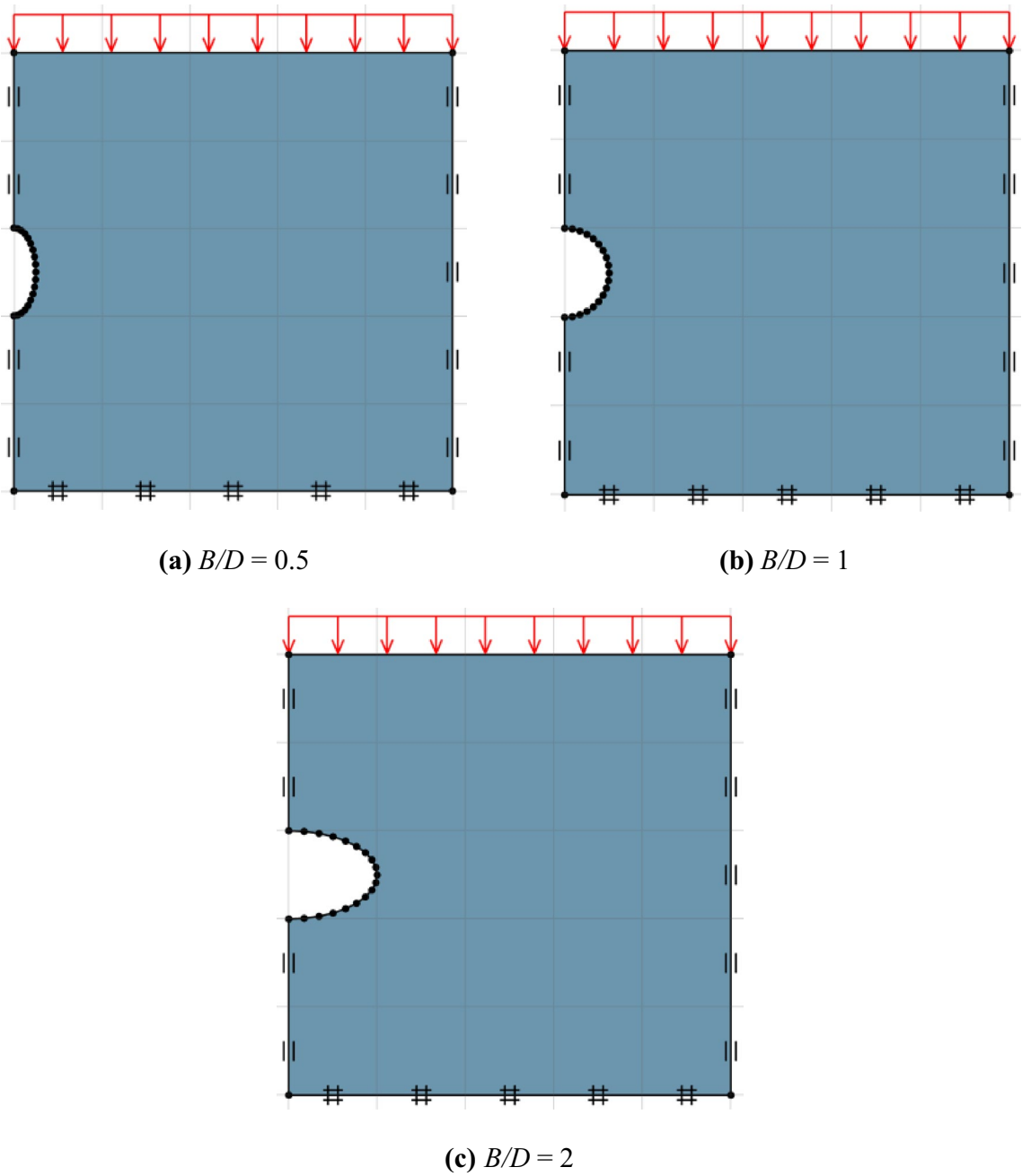

(a) $B/D = 0.5$ **(b)** $B/D = 1$

(c) $B/D = 2$

Fig. 2 Model geometry for three unlined elliptical tunnels in rock mass

in-situ condition is applicable to the HB model with the disturbance factor DF be set to zero. This leads to the six design parameters in this study (i.e., B, D, σ_{ci}, GSI, m_i, γ). Using the dimensionless output parameter (σ_s/σ_{ci}), where σ_s is the uniform surcharge at collapse, Eq. (6) defines the stability factor (σ_s/σ_{ci}) that can be written as a function of five dimensionless parameters:

$$\frac{\sigma_s}{\sigma_{ci}} = f\left(\frac{B}{D}, \frac{C}{D}, \frac{\sigma_{ci}}{\gamma D}, m_i, \text{GSI}\right), \tag{6}$$

where B/D is the width ratio and C/D denotes the cover depth ratio. $\sigma_{ci}/\gamma D$ represents the normalized uniaxial compressive strength ratio. σ_s/σ_{ci} is the stability factor. The parametric ranges considered in the current stability study are: (1). the cover depth ratio of tunnels is $C/D = 1$—5; (2). the width ratio is $B/D = 0.5$–2; (3). the yield parameter m_i for the frictional strength of intact rock mass is $m_i = 5$–30;

(4). The geological strength index is $GSI = 40–100$, and the dimensionless uniaxial compressive strength ratio $\sigma_{ci}/\gamma D$ is set to be 100–∞. Note that $\sigma_{ci}/\gamma D = \infty$ corresponds to a rock mass with extremely high strength (either σ_{ci} is very large or γ is very small). The practical ranges of dimensionless parameters were chosen by following the previous research in the stability of other tunnel shapes in rock masses (e.g., Keawsawasvong and Ukritchon 2020; Ukritchon and Keawsawasvong 2019a, b; Xiao et al. 2019, 2021; Zhang et al. 2019).

2.1.1 Limitations

The rock masses in this study are defined to obey the Hoek–Brown (HB) failure criterion version 2002 (Hoek et al. 2002), where the considered parameters and their ranges include the yield parameter $m_i = 5–30$, the geological strength index GSI = 40–100, and the dimensionless uniaxial compressive strength ratio $\sigma_{ci}/\gamma D = 100–\infty$. The study assumes an excellent quality-controlled blasting or excavation by tunnel boring machine (TBM) during the tunnel construction. In this aspect, the disturbance factor (DF) of the

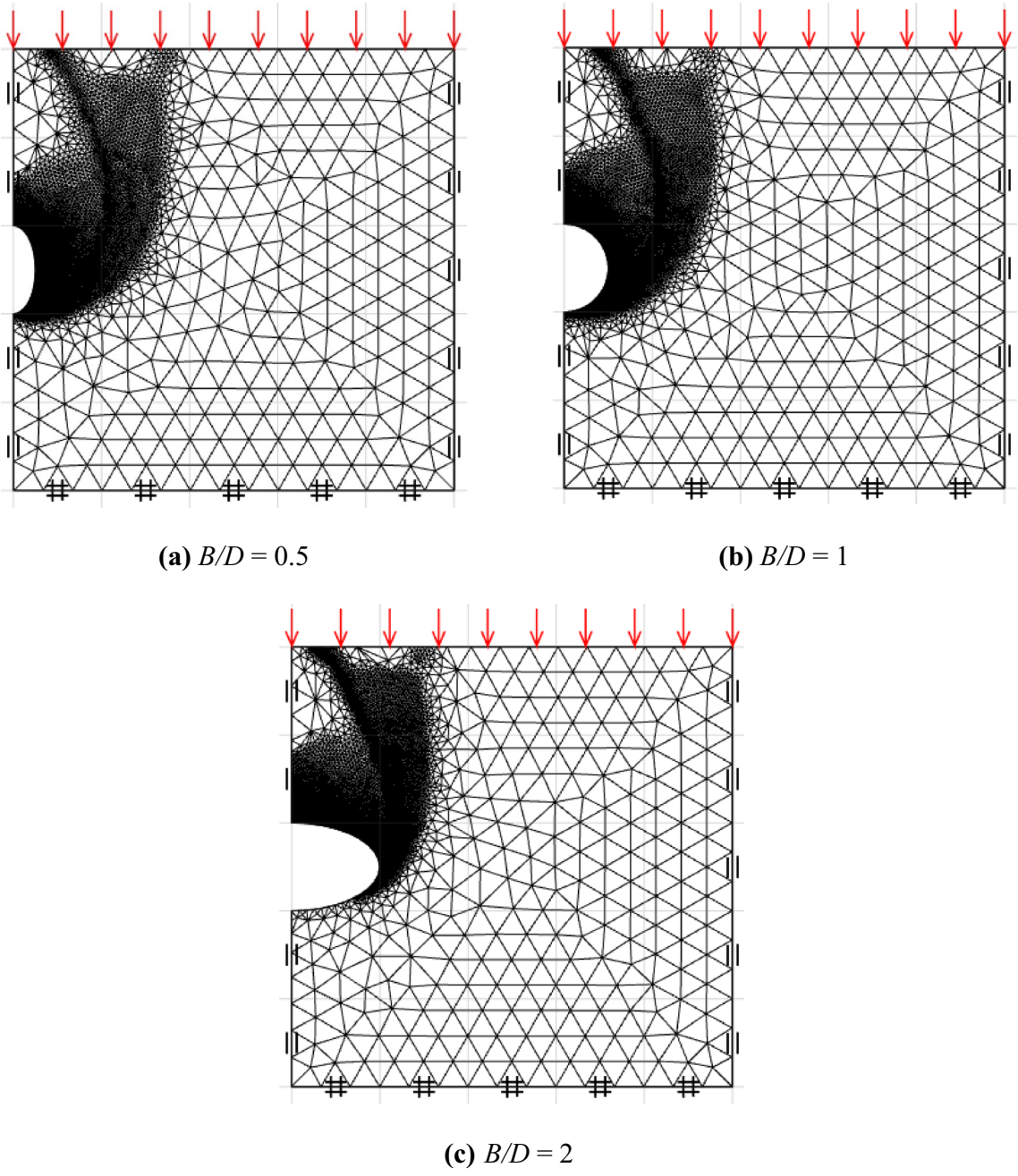

(a) $B/D = 0.5$ **(b)** $B/D = 1$

(c) $B/D = 2$

Fig. 3 Typical adaptive meshes of unlined elliptical tunnel in rock mass

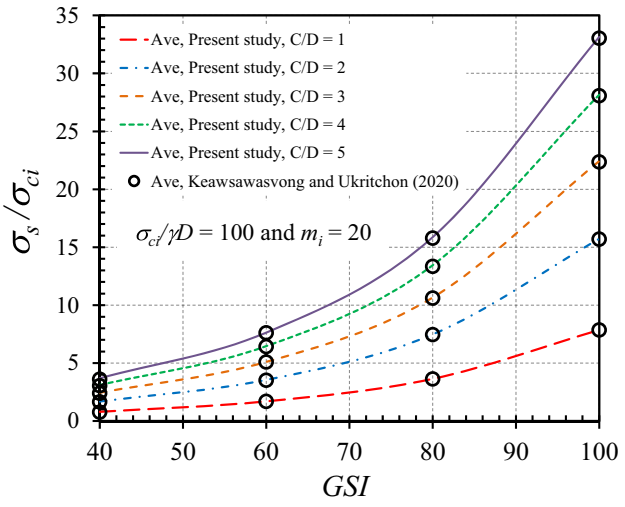

Fig. 4 Comparison of the stability factors σ_s/σ_{ci} ($B/D = 1$, i.e., circular tunnel)

confined rock mass surrounding a tunnel can be considered as very low or close to zero (DF = 0). More information on the guidelines for estimating the proper number of the disturbance factor (DF) can be found in Hoek et al. (2002). An example showing the effect of the disturbance factor on the tunnel stability can be found in Xiao et al. (2021).

In addition, the cover depth ratio of tunnels is limited to the cases of $C/D = 1$–5 and the width ratio is limited to the cases of $B/D = 0.5$–2 in this study. It should be also noted that, when the uniaxial compressive strength is very small (or almost zero), it corresponding to highly fractured rock masses and the HB failure criterion does present certain limitation in the present stability analysis.

2.2 FELA Modelling

The proposed computational limit analysis is based on the theoretical work presented in Sloan (2013). It employs plastic bounding theorems, finite element discretization, and nonlinear programming. The associated upper and lower bound theorems (UB and LB) follow a perfectly plastic material with an associated flow rule. It is expected that a true stability solution can be bracketed from above (UB) and below (LB). A new computer program OptumG2 (OptumCE 2020) has been widely used to solve several geotechnical stability problems (e.g., Shiau and Smith 2006; Shiau et al. 2006a, b, 2021, Shiau and Al-Asadi 2018; 2020a, b, c, 2021; Ukritchon and Keawsawasvong 2017; Keawsawasvong and Ukritchon 2020). The program is, therefore, selected in this paper to compute the active collapse of unlined elliptical tunnels in rock masses using the latest powerful adaptivity meshing technique.

Using the model domains under plane strain conditions (see Fig. 2), three typical FELA meshes are shown in Fig. 3. The symmetrical plane on the left-hand side has a boundary condition that allows vertical movement only. This boundary condition is also applied to the right-hand side boundary of the domain. At the bottom plane, the boundary condition is set to be no movements in both vertical and horizontal directions. It is important to ensure that no error occurred in the computed bound solutions due to the problem size. Therefore, the sizes of the domain are carefully chosen to be so large that there is no intersection of the plastic shear zone at the far side and the bottom boundaries. The nodes on the periphery of the tunnel are free to move and there is no internal pressure presented inside the tunnel. The mesh adaptivity feature proposed by Ciria et al. (2008) is employed in this study. Using this powerful feature, a large number of elements can be automatically generated in zones where plastic shear strains are high. Throughout the study of the paper, five iterations of mesh adaptivity and 10,000 elements for the final mesh were set for all analyses.

The compressive uniform surcharge σ_s is applied on the rock surface and it is the main objective function to be optimized at the active collapse state. The upper bound solution of the problem is obtained by solving the optimization problem that minimizes the surcharge (σ_s) (i.e., the objective function) and is subjected to the kinematically admissible velocity constraints. For the calculations of a lower bound solution, it is achieved by solving the optimization problem that maximizes the surcharge pressure (σ_s) (i.e., the objective function), while subjecting to the statically admissible stress constraints including equilibrium equations within the elements and along stress discontinuities, stress boundary conditions, and nowhere violation of the HB failure criterion. Once the surcharge pressure (σ_s) is computed for each parametric analysis, Eq. (6) is then used to calculate the stability factor (σ_s/σ_{ci}).

3 Comparison of Results

Since the differences between UB and LB solutions obtained in this study are within an acceptable limit of 5%, all numerical results are hereafter presented as the average solutions (Ave) of the upper bound (UB) and lower bound (LB). In spite of this confidence in numerical results, Fig. 4 still shows a comparison of stability factor (σ_s/σ_{ci}) between the present study and that of Keawsawasvong and Ukritchon (2020). The selected cases for the comparison are: $B/D = 1$; $m_i = 20$; $\sigma_{ci}/\gamma D = 100$; $C/D = 1, 2, 3, 4, 5$; $GSI = 40, 60, 80, 100$. It is positive to see the excellent agreement between the two solutions, further giving great confidence before

Table 1 Stability factors σ_s/σ_{ci} for elliptical tunnels ($B/D=0.5$)

$\sigma_{ci}/\gamma D$	C/D	m_i	GSI = 40	GSI = 60	GSI = 80	GSI = 100
100	1	5	0.313	0.762	1.756	4.127
		10	0.607	1.383	3.032	6.706
		20	1.213	2.632	5.569	11.910
		30	1.830	3.886	8.114	16.914
	2	5	0.552	1.302	2.918	6.636
		10	1.098	2.436	5.242	11.352
		20	2.220	4.713	9.858	20.652
		30	3.374	7.002	14.445	30.048
	3	5	0.752	1.750	3.885	8.723
		10	1.510	3.320	7.089	15.195
		20	3.071	6.459	13.438	28.101
		30	4.669	9.631	19.764	40.961
	4	5	0.920	2.132	4.711	10.494
		10	1.864	4.062	8.679	18.522
		20	3.794	7.974	16.499	34.504
		30	5.785	11.879	24.378	50.209
	5	5	1.068	2.464	5.420	12.051
		10	2.176	4.733	10.091	21.410
		20	4.451	9.292	19.196	40.102
		30	6.776	13.882	28.401	58.491
1000	1	5	0.331	0.780	1.778	4.134
		10	0.628	1.398	3.039	6.696
		20	1.236	2.647	5.598	11.905
		30	1.852	3.902	8.089	16.982
	2	5	0.582	1.331	2.945	6.662
		10	1.129	2.471	5.280	11.411
		20	2.251	4.752	9.881	20.757
		30	3.403	7.043	14.473	30.087
	3	5	0.793	1.794	3.929	8.757
		10	1.557	3.363	7.135	15.216
		20	3.118	6.502	13.491	28.168
		30	4.710	9.674	19.793	40.996
	4	5	0.977	2.186	4.766	10.546
		10	1.923	4.125	8.719	18.583
		20	3.860	8.030	16.552	34.547
		30	5.843	11.934	24.451	50.399
	5	5	1.136	2.527	5.480	12.083
		10	2.243	4.801	10.102	21.425
		20	4.512	9.367	19.275	40.148
		30	6.850	13.912	28.439	58.699
∞	1	5	0.333	0.782	1.776	4.144
		10	0.629	1.399	3.049	6.729
		20	1.233	2.651	5.576	11.939
		30	1.854	3.899	8.126	16.920
	2	5	0.585	1.334	2.947	6.643
		10	1.134	2.470	5.279	11.409
		20	2.262	4.758	9.861	20.733
		30	3.403	7.039	14.471	30.058

Table 1 (continued)

$\sigma_{ci}/\gamma D$	C/D	m_i	GSI = 40	GSI = 60	GSI = 80	GSI = 100
	3	5	0.797	1.791	3.931	8.762
		10	1.561	3.359	7.141	15.252
		20	3.125	6.513	13.455	28.125
		30	4.712	9.685	19.801	40.980
	4	5	0.982	2.190	4.761	10.552
		10	1.927	4.134	8.721	18.569
		20	3.868	8.023	16.566	34.577
		30	5.852	11.936	24.423	50.427
	5	5	1.143	2.537	5.501	12.095
		10	2.254	4.798	10.140	21.435
		20	4.524	9.356	19.261	40.179
		30	6.839	13.935	28.467	58.655

producing the comprehensive design charts, tables, and equations in the next section.

4 Stability Charts and Tables

A total of 1,200 computed solutions (Ave) of the stability factor (σ_s/σ_{ci}) are presented in Tables 1, 2, 3, 4, 5 for $B/D = (0.5, 0.75, 1, 1.333, \text{and } 2)$. Numerical results of the stability factor are also presented graphically in Figs. 5, 6, 7, 8, 9 to study the individual effect of the considered parameters (e.g., B/D, C/D, $\sigma_{ci}/\gamma D$, GSI, and m_i).

Figure 5a and b presents the effect of *GSI* on the stability factor (σ_s/σ_{ci}) for various values of B/D. The data of the plots are for $C/D = 3$, $\sigma_{ci}/\gamma D = 1000$, and $m_i = 5$ and 30, respectively. Numerical results have shown an exponential relationship between GSI and σ_s/σ_{ci}, where an increase of GSI results in a nonlinear increase of σ_s/σ_{ci} for all B/D. This observation is compatible with the exponential function of the HB failure criterion in Eqs. (2)–(4).

The effect of m_i on σ_s/σ_{ci} is illustrated in Fig. 6a and b for the cases of GSI = 40 and 100, respectively. The plots are for ($C/D = 3$, $\sigma_{ci}/\gamma D = 1000$) and for five different width ratios $B/D = (0.5, 0.75, 1, 1.333, \text{and } 2)$. Numerical results have shown a linear relationship between σ_s/σ_{ci} and m_i. Figure 7a and b presents the effect of $\sigma_{ci}/\gamma D$ on σ_s/σ_{ci} for $m_i = 5$ and 30, respectively. The plot is for the case of $C/D = 3$ and GSI = 80, and it is concluded that $\sigma_{ci}/\gamma D$ has little to no effect on the stability factor σ_s/σ_{ci}. This is not dissimilar to the undrained stability problems in soils, in which the normalized strength ratio has a negligible effect on the overall stability of rock tunnels too (Shiau and Al-Asadi 2018). The effect of cover depth ratio C/D on σ_s/σ_{ci} is shown in Fig. 8a and b, respectively, for $m_i = 5$ and 30. A nonlinear relationship between C/D and σ_s/σ_{ci} exists. A larger C/D value results in greater stability (σ_s/σ_{ci}). Finally, Fig. 9a and b depicts the influence of B/D on σ_s/σ_{ci} for $m_i = 5$ and 30, respectively. The plots are for five different values of $C/D = 1$–5. Numerical results have shown a nonlinear decrease in the stability factor σ_s/σ_{ci} with the increasing B/D. A larger B/D ratio results in a smaller value of σ_s/σ_{ci}, which is in line with common engineering judgment.

Table 2 Stability factors σ_s/σ_{ci} for elliptical tunnels ($B/D = 0.75$)

$\sigma_{ci}/\gamma D$	C/D	m_i	GSI = 40	$GSI = 60$	$GSI = 80$	$GSI = 100$
100	1	5	0.256	0.633	1.474	3.481
		10	0.491	1.134	2.501	5.584
		20	0.980	2.151	4.577	9.812
		30	1.480	3.169	6.625	13.909
	2	5	0.479	1.142	2.593	5.929
		10	0.953	2.129	4.616	10.036
		20	1.923	4.109	8.663	18.141
		30	2.915	6.108	12.599	26.309
	3	5	0.666	1.564	3.497	7.879
		10	1.340	2.961	6.368	13.738
		20	2.723	5.773	11.973	25.173
		30	4.124	8.575	17.646	36.605
	4	5	0.825	1.928	4.285	9.585
		10	1.673	3.672	7.866	16.798
		20	3.412	7.189	14.896	31.207
		30	5.196	10.673	21.960	45.513
	5	5	0.964	2.241	4.954	11.052
		10	1.963	4.301	9.156	19.557
		20	4.017	8.415	17.415	36.408
		30	6.131	12.575	25.776	53.161
1000	1	5	0.274	0.650	1.489	3.496
		10	0.512	1.150	2.527	5.596
		20	1.004	2.174	4.598	9.846
		30	1.509	3.192	6.635	13.952
	2	5	0.512	1.172	2.618	5.938
		10	0.987	2.160	4.642	10.058
		20	1.959	4.145	8.711	18.208
		30	2.954	6.145	12.600	26.289
	3	5	0.711	1.607	3.548	7.939
		10	1.386	3.005	6.400	13.778
		20	2.773	5.807	12.025	25.223
		30	4.191	8.603	17.672	36.729
	4	5	0.883	1.985	4.338	9.625
		10	1.731	3.728	7.929	16.856
		20	3.451	7.233	14.960	31.281
		30	5.257	10.733	22.042	45.539
	5	5	1.033	2.310	5.005	11.111
		10	2.038	4.363	9.223	19.590
		20	4.098	8.509	17.523	36.423
		30	6.198	12.602	25.827	53.236
∞	1	5	0.276	0.651	1.490	3.496
		10	0.516	1.157	2.530	5.593
		20	1.007	2.172	4.595	9.848
		30	1.512	3.191	6.616	13.927
	2	5	0.514	1.175	2.621	5.948
		10	0.993	2.159	4.637	10.062
		20	1.957	4.154	8.651	18.174
		30	2.951	6.150	12.620	26.350

Table 2 (continued)

$\sigma_{ci}/\gamma D$	C/D	m_i	GSI = 40	$GSI = 60$	$GSI = 80$	$GSI = 100$
	3	5	0.713	1.618	3.5515	7.933
		10	1.389	3.004	6.409	13.754
		20	2.777	5.821	12.058	25.257
		30	4.195	8.603	17.7025	36.732
	4	5	0.888	1.991	4.3425	9.630
		10	1.738	3.733	7.916	16.870
		20	3.483	7.243	14.934	31.296
		30	5.262	10.746	22.041	45.584
	5	5	1.040	2.314	5.010	11.102
		10	2.045	4.372	9.248	19.594
		20	4.102	8.485	17.524	36.558
		30	6.212	12.677	25.847	53.393

Table 3 Stability factors σ_s/σ_{ci} for elliptical tunnels ($B/D = 1$)

$\sigma_{ci}/\gamma D$	C/D	m_i	GSI = 40	GSI = 60	GSI = 80	GSI = 100
100	1	5	0.200	0.508	1.196	2.850
		10	0.387	0.905	2.022	4.515
		20	0.796	1.701	3.647	7.865
		30	1.158	2.513	5.294	11.200
	2	5	0.409	0.990	2.264	5.210
		10	0.815	1.841	4.000	8.755
		20	1.686	3.548	7.476	15.725
		30	2.500	5.255	10.914	22.788
	3	5	0.584	1.392	3.136	7.110
		10	1.180	2.629	5.664	12.226
		20	2.449	5.101	10.662	22.433
		30	3.652	7.576	15.689	32.598
	4	5	0.736	1.740	3.884	8.718
		10	1.494	3.303	7.073	15.217
		20	3.108	6.459	13.446	28.146
		30	4.644	9.604	19.763	40.906
	5	5	0.866	2.035	4.528	10.118
		10	1.770	3.895	8.320	17.771
		20	3.695	7.634	15.870	33.143
		30	5.526	11.369	23.344	48.338
1000	1	5	0.219	0.523	1.211	2.867
		10	0.408	0.921	2.035	4.530
		20	0.796	1.725	3.675	7.898
		30	1.186	2.524	5.313	11.248
	2	5	0.443	1.022	2.291	5.218
		10	0.850	1.870	4.037	8.775
		20	1.686	3.582	7.506	15.768
		30	2.538	5.294	10.962	22.802

Table 3 (continued)

$\sigma_{ci}/\gamma D$	C/D	m_i	GSI = 40	GSI = 60	GSI = 80	GSI = 100
	3	5	0.631	1.438	3.179	7.147
		10	1.224	2.674	5.686	12.340
		20	2.451	5.145	10.687	22.470
		30	3.702	7.641	15.687	32.614
	4	5	0.793	1.794	3.935	8.790
		10	1.556	3.357	7.142	15.273
		20	3.109	6.506	13.451	28.193
		30	4.705	9.683	19.838	40.956
	5	5	0.935	2.107	4.589	10.168
		10	1.838	3.960	8.398	17.883
		20	3.697	7.707	15.904	33.195
		30	5.594	11.445	23.397	48.382
∞	1	5	0.221	0.527	1.213	2.868
		10	0.411	0.926	2.035	4.533
		20	0.800	1.726	3.665	7.904
		30	1.194	2.536	5.314	11.222
	2	5	0.445	1.019	2.293	5.232
		10	0.853	1.878	4.043	8.790
		20	1.691	3.577	7.521	15.774
		30	2.543	5.299	10.953	22.824
	3	5	0.635	1.441	3.179	7.146
		10	1.234	2.676	5.710	12.324
		20	2.454	5.158	10.721	22.475
		30	3.706	7.662	15.764	32.622
	4	5	0.796	1.800	3.941	8.807
		10	1.559	3.367	7.155	15.265
		20	3.122	6.517	13.469	28.209
		30	4.714	9.683	19.828	40.965
	5	5	0.944	2.110	4.604	10.176
		10	1.852	3.966	8.412	17.905
		20	3.689	7.716	15.902	33.214
		30	5.612	11.467	23.364	48.431

Figure 10 compares the failure mechanisms of three $B/D = 0.5$, 1, and 2. In general, the failure zone of unlined elliptical tunnels is in the form of an elliptical shape beginning from the rock surface to the base of the tunnel. It is also interesting to see that, as B/D increases from 0.5 to 2, the ending point of the failure surface inside the tunnel has moved from the base of the tunnel to somewhere near the mid-height of the tunnel. Noting that the absolute values of shear dissipation are not important in such a perfect plasticity model, they are not presented in the figure. The depth ratio effects ($C/D = 1$, 2, 4, 5) on the overall failure mechanisms of the three various width ratios ($B/D = 0.5$, 1, and 2) are shown in Figs. 11, 12, 13, respectively. The plots are for $\sigma_{ci}/\gamma D = 1000$, GSI = 80, and $m_i = 20$. A larger C/D results in a greater spreading of the failure zone around the tunnel, given the current study under the surcharge effects. For all cases presented, the failure zones extend to the base of tunnels when $C/D \geq 2$.

Table 4 Stability factors σ_s/σ_{ci} for elliptical tunnels ($B/D = 1.333$)

$\sigma_{ci}/\gamma D$	C/D	m_i	GSI = 40	GSI = 60	GSI = 80	GSI = 100
100	1	5	0.138	0.363	0.875	2.108
		10	0.268	0.643	1.454	3.291
		20	0.538	1.200	2.608	5.662
		30	0.809	1.774	3.767	8.028
	2	5	0.325	0.808	1.867	4.342
		10	0.649	1.489	3.258	7.206
		20	1.320	2.870	6.086	12.945
		30	1.997	4.251	8.869	18.534
	3	5	0.488	1.187	2.700	6.182
		10	0.987	2.228	4.836	10.508
		20	2.013	4.317	9.076	19.115
		30	3.047	6.433	13.313	27.746
	4	5	0.627	1.509	3.402	7.713
		10	1.280	2.860	6.161	13.383
		20	2.630	5.597	11.660	24.465
		30	3.981	8.308	17.130	35.642
	5	5	0.748	1.789	4.022	9.054
		10	1.536	3.416	7.349	15.782
		20	3.156	6.688	13.958	29.196
		30	4.804	9.980	20.435	42.571
1000	1	5	0.157	0.382	0.891	2.131
		10	0.290	0.663	1.472	3.304
		20	0.562	1.230	2.629	5.682
		30	0.839	1.803	3.779	8.039
	2	5	0.360	0.839	1.897	4.359
		10	0.689	1.529	3.317	7.256
		20	1.361	2.904	6.119	12.938
		30	2.035	4.289	8.905	18.602
	3	5	0.538	1.233	2.751	6.212
		10	1.041	2.279	4.880	10.595
		20	2.068	4.381	9.135	19.151
		30	3.123	6.478	13.357	27.777
	4	5	0.689	1.570	3.462	7.772
		10	1.344	2.924	6.235	13.450
		20	2.688	5.644	11.707	24.551
		30	4.056	8.389	17.238	35.727
	5	5	0.822	1.865	4.079	9.120
		10	1.616	3.481	7.412	15.865
		20	3.239	6.767	14.003	29.265
		30	4.894	10.045	20.564	42.601
∞	1	5	0.137	0.383	0.893	2.129
		10	0.269	0.665	1.472	3.310
		20	0.566	1.236	2.632	5.673
		30	0.843	1.805	3.793	8.040
	2	5	0.325	0.843	1.899	4.363
		10	0.650	1.533	3.317	7.260
		20	1.367	2.916	6.124	12.987
		30	2.053	4.302	8.916	18.574

Table 4 (continued)

$\sigma_{ci}/\gamma D$	C/D	m_i	GSI = 40	GSI = 60	GSI = 80	GSI = 100
	3	5	0.488	1.233	2.751	6.224
		10	0.987	2.284	4.893	10.584
		20	2.077	4.385	9.123	19.156
		30	3.131	6.486	13.383	27.810
	4	5	0.627	1.573	3.472	7.784
		10	1.280	2.925	6.230	13.448
		20	2.696	5.653	11.717	24.542
		30	4.072	8.373	17.242	35.706
	5	5	0.748	1.868	4.080	9.121
		10	1.536	3.493	7.417	15.859
		20	3.243	6.767	14.011	29.292
		30	4.904	10.030	20.589	42.463

A quick comparison of the stability factors σ_s/σ_{ci} for the different shapes of tunnels is shown in Fig. 14. Two published results are considered in the comparison, and they are for the square tunnel (Ukritchon and Keawsawasvong 2019a) and the plane strain heading (Ukritchon and Keawsawasvong 2019b). Together with our elliptical tunnels ($B/D = 0.5$ and 2) and circular tunnels ($B/D = 1$), numerical results have shown that the stability factors σ_s/σ_{ci} of plane strain heading is the largest, and it is then followed by the elliptical tunnel with $B/D = 0.5$, the circular tunnel $B/D = 1$, the square tunnel, and the elliptical tunnel with $B/D = 2$. This comparison figure is useful and is of great value to design practitioners in making engineering decisions.

4.1 Stability Equations

Using the average stability solutions (Ave) of upper and lower bounds and a curve fitting method, several design equations are developed to estimate the stability factor σ_s/σ_{ci} of shallow unlined horseshoe tunnels in Hoek–Brown rock masses. The mathematical form of approximate expressions based on Keawsawasvong and Ukritchon (2020) are expressed in the following equations:

$$\frac{\sigma_s}{\sigma_{ci}} = F_1 + F_2 m_i - F_3\left(\frac{\gamma D}{\sigma_{ci}}\right), \tag{7a}$$

$$F_1 = GSI\left[b_1 + b_2\frac{C}{D} + b_3\left(\frac{C}{D}\right)^2\right] + GSI^2\left[c_1 + c_2\frac{C}{D} + c_3\left(\frac{C}{D}\right)^2\right], \tag{7b}$$

$$F_2 = e_1 + e_2\frac{C}{D} + GSI\left[f_1 + f_2\frac{C}{D} + f_3\left(\frac{C}{D}\right)^2\right] + GSI^2\left[g_1 + g_2\frac{C}{D}\right] + GSI^3\left(d_1\frac{C}{D}\right), \tag{7c}$$

$$F_3 = a_1 + a_2\frac{C}{D}, \tag{7d}$$

where (a_i, b_i, c_i, d_i, e_i, f_i, and g_i) are constant coefficients for the equations. The least-square method proposed by Sauer (2014) was used to determine the optimal values of the constant coefficients. Sauer's method can be used to minimize the sum of squares of the deviation (i.e., the error) in the stability factor (σ_s/σ_{ci}) between the computed Ave solutions and the approximate solutions (i.e., the predictions). The comprehensive constants so obtained for the design Eqs. (7a)–(7d) are shown in Table 6 for width ratios $B/D = 0.5$, 0.75, 1, 1.33, and 2. The coefficient of determination (R^2) for each B/D equation is approximately 99.98%, indicating a very high precision of the developed constants and equations, which can be further used with great confidence by practitioners to estimate the stability factor σ_s/σ_{ci} of shallow unlined elliptical tunnels in rock masses.

Table 5 Stability factors σ_s/σ_{ci} for elliptical tunnels ($B/D=2$)

$\sigma_{ci}/\gamma D$	C/D	m_i	GSI = 40	GSI = 60	GSI = 80	GSI = 100
100	1	5	0.059	0.180	0.457	1.156
		10	0.117	0.312	0.726	1.701
		20	0.240	0.580	1.265	2.834
		30	0.355	0.849	1.840	3.971
	2	5	0.190	0.513	1.221	2.901
		10	0.387	0.944	2.108	4.708
		20	0.796	1.812	3.889	8.360
		30	1.146	2.685	5.652	11.960
	3	5	0.326	0.844	1.966	4.565
		10	0.668	1.581	3.482	7.672
		20	1.394	3.063	6.511	13.824
		30	2.102	4.564	9.515	19.931
	4	5	0.449	1.137	2.621	6.026
		10	0.931	2.152	4.701	10.282
		20	1.919	4.194	8.841	18.730
		30	2.980	6.242	12.962	27.042
	5	5	0.557	1.394	3.191	7.282
		10	1.161	2.654	5.770	12.557
		20	2.504	5.185	10.876	22.935
		30	3.410	7.704	15.997	33.311
1000	1	5	0.079	0.195	0.470	1.170
		10	0.141	0.329	0.750	1.716
		20	0.269	0.605	1.306	2.852
		30	0.398	0.875	1.861	4.001
	2	5	0.231	0.548	1.254	2.929
		10	0.437	0.983	2.148	4.748
		20	0.861	1.857	3.926	8.367
		30	1.293	2.738	5.685	11.979
	3	5	0.386	0.895	2.016	4.586
		10	0.741	1.641	3.534	7.740
		20	1.467	3.129	6.566	13.899
		30	2.209	4.631	9.573	19.987
	4	5	0.523	1.202	2.679	6.094
		10	1.013	2.217	4.765	10.349
		20	2.014	4.267	8.942	18.735
		30	3.041	6.329	13.022	27.140
	5	5	0.644	1.469	3.260	7.321
		10	1.253	2.733	5.847	12.626
		20	2.500	5.278	10.958	23.022
		30	3.777	7.806	16.076	33.412
∞	1	5	0.081	0.198	0.473	1.171
		10	0.143	0.333	0.751	1.708
		20	0.272	0.606	1.305	2.855
		30	0.405	0.878	1.861	3.998
	2	5	0.235	0.552	1.258	2.931
		10	0.441	0.989	2.148	4.752
		20	0.867	1.860	3.931	8.384
		30	1.298	2.737	5.702	11.991

Table 5 (continued)

$\sigma_{ci}/\gamma D$	C/D	m_i	GSI = 40	GSI = 60	GSI = 80	GSI = 100
	3	5	0.391	0.902	2.022	4.621
		10	0.748	1.645	3.550	7.732
		20	1.475	3.138	6.581	13.908
		30	2.215	4.636	9.590	19.997
	4	5	0.530	1.209	2.687	6.089
		10	1.021	2.228	4.772	10.360
		20	2.026	4.284	8.917	18.738
		30	3.047	6.316	13.062	27.113
	5	5	0.652	1.479	3.272	7.353
		10	1.263	2.742	5.849	12.629
		20	2.516	5.280	10.948	23.001
		30	3.787	7.819	16.103	33.439

5 Example

The practical use of the proposed equations is best explained using an example. The selected example of an elliptical tunnel has a horizontal dimension $B = 6$ m, a vertical dimension $D = 3$ m, a cover depth $C = 3$ m. The rock is found to have GSI = 50, $m_i = 17$, $\sigma_{ci} = 63$ MPa, and $\gamma = 22$ kN/m^3. Determine the maximum surcharge pressure (σ_s) allowed before the tunnel reaches a collapse state.

1. Calculating $B/D = 6/3 = 2$, $C/D = 3/3 = 1$, and $\gamma D/\sigma_{ci} = 22^*3/63{,}000 = 0.001$.
2. Based on the value of $B/D = 2$, the constant coefficients including a_1, a_2, b_1, b_2, b_3, c_1, c_2, c_3, d_1, e_1, e_2, f_1, f_2, f_3, g_1, and g_2 can be obtained using Table 6.
3. Substituted all parameters including C/D, $\gamma D/\sigma_{ci}$, GSI, m_i, and a_1 to g_2 into Eqs. (7a)–(7d), σ_s/σ_{ci} can be then obtained as: $\sigma_s/\sigma_{ci} = 0.372$.
4. The maximum surcharge pressure is calculated as $\sigma_s = 120^*0.372 = 42.38$ MPa.

6 Conclusions

To the best of the authors' knowledge, there was no published stability solution for unlined elliptical tunnels in Hoek–Brown rock masses. With the advanced adaptive meshing technique, finite elements, and nonlinear programming, this paper has successfully studied the stability of unlined elliptical tunnel in Hoek–Brown rock mass under the effect of surcharge pressure. Both the upper and lower bound limit analyses were used to solve for the stability solutions of a wide range of geometrical and Hoek–Brown material parameters. Using the average bound solutions, new design equations for computing the stability factors were developed using a least-square method. The proposed design equations are accurate with the coefficient of determination $R^2 = 99.98\%$. This paper provides information that can be used as a reference at the preliminary design stage.

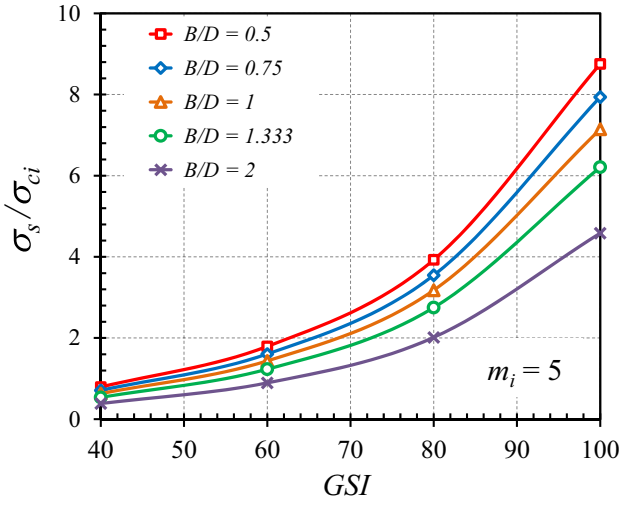

(a) $m_i = 5$

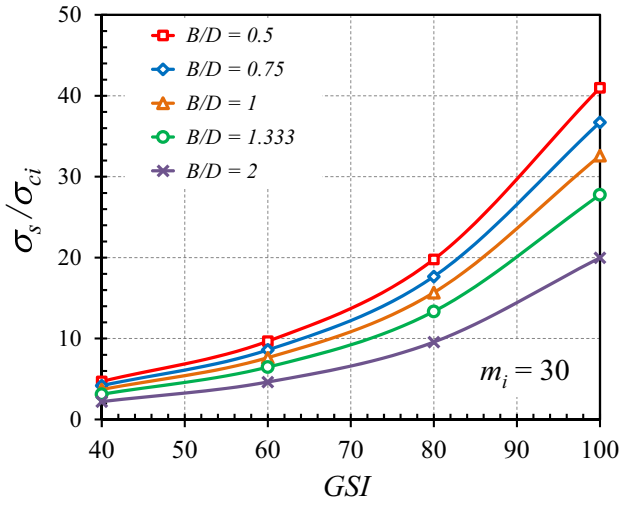

(b) $m_i = 30$

Fig. 5 Influence of GSI on the stability factors σ_s/σ_{ci} ($C/D = 3$ and $\sigma_{ci}/\gamma D = 1000$)

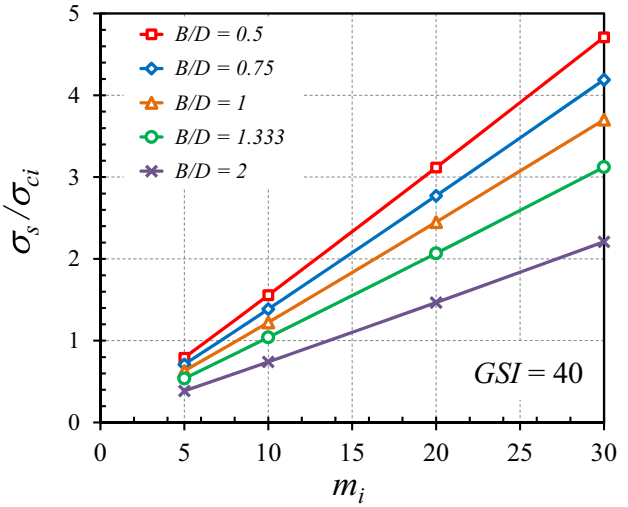

(a) $GSI = 4$

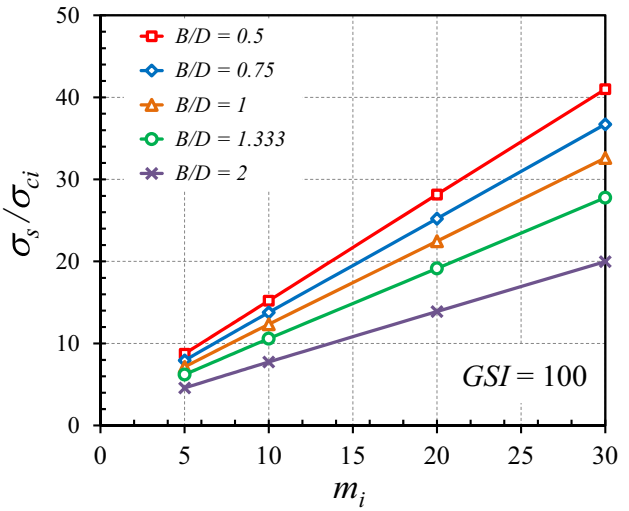

(b) $GSI = 100$

Fig. 6 Influence of m_i on the stability factors σ_s/σ_{ci} ($C/D = 3$ and $\sigma_{ci}/\gamma D = 1000$)

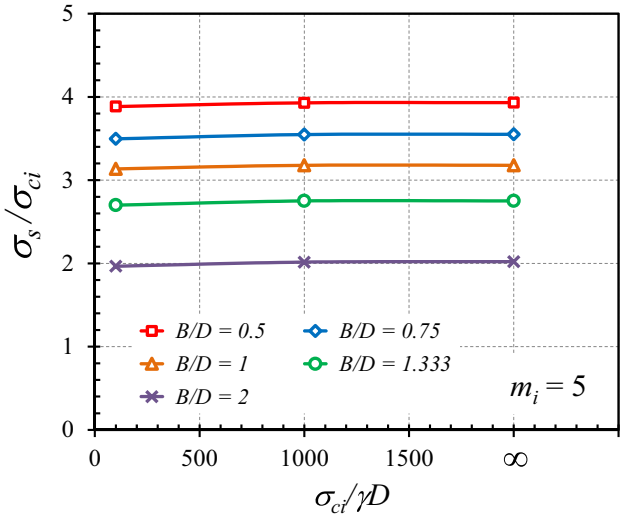

(a) $m_i = 5$

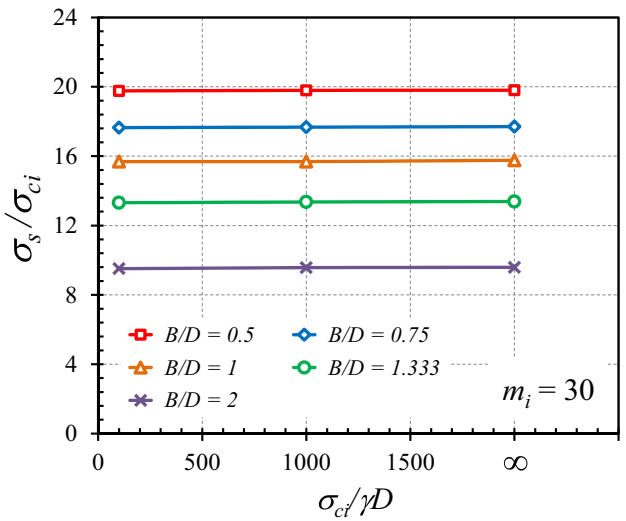

(b) $m_i = 30$

Fig. 7 Influence of $\sigma_{ci}/\gamma D$ on the stability factors σ_s/σ_{ci} ($C/D = 3$ and GSI = 80)

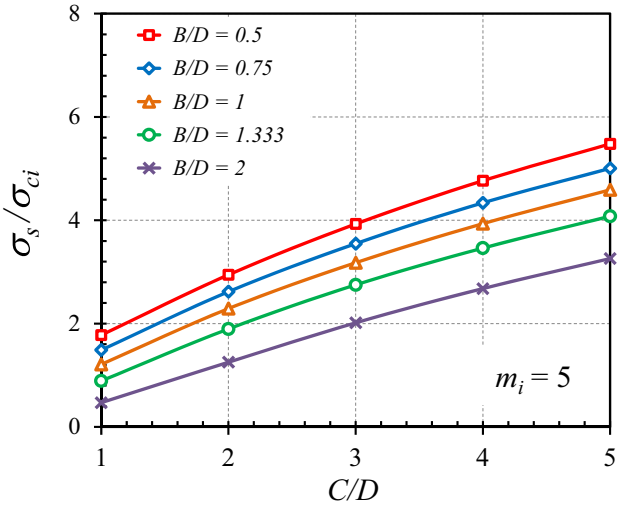

(a) $m_i = 5$

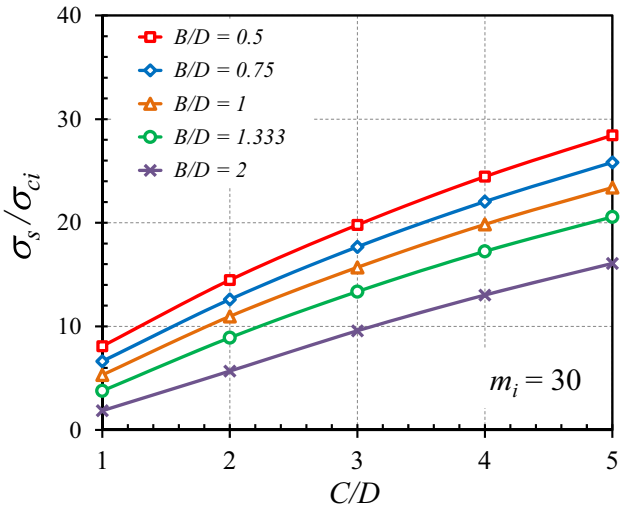

(b) $m_i = 30$

Fig. 8 Influence of C/D on the stability factors σ_s/σ_{ci} ($\sigma_{ci}/\gamma D = 1000$ and GSI = 80)

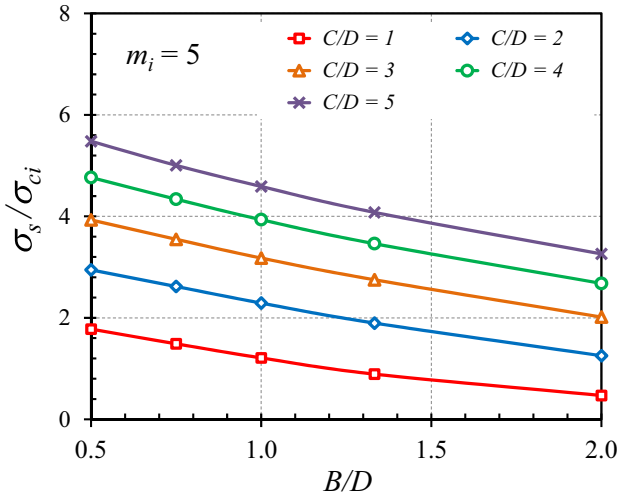

(a) $m_i = 5$

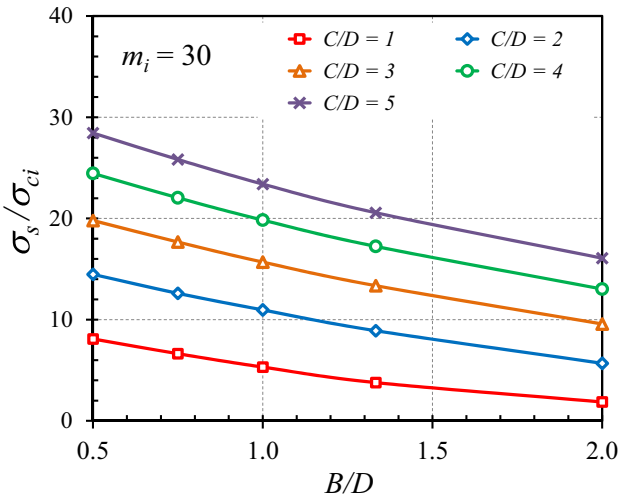

(b) $m_i = 30$

Fig. 9 Influence of *B/D* on the stability factors σ_s/σ_{ci} ($\sigma_{ci}/\gamma D = 1000$ and GSI = 80)

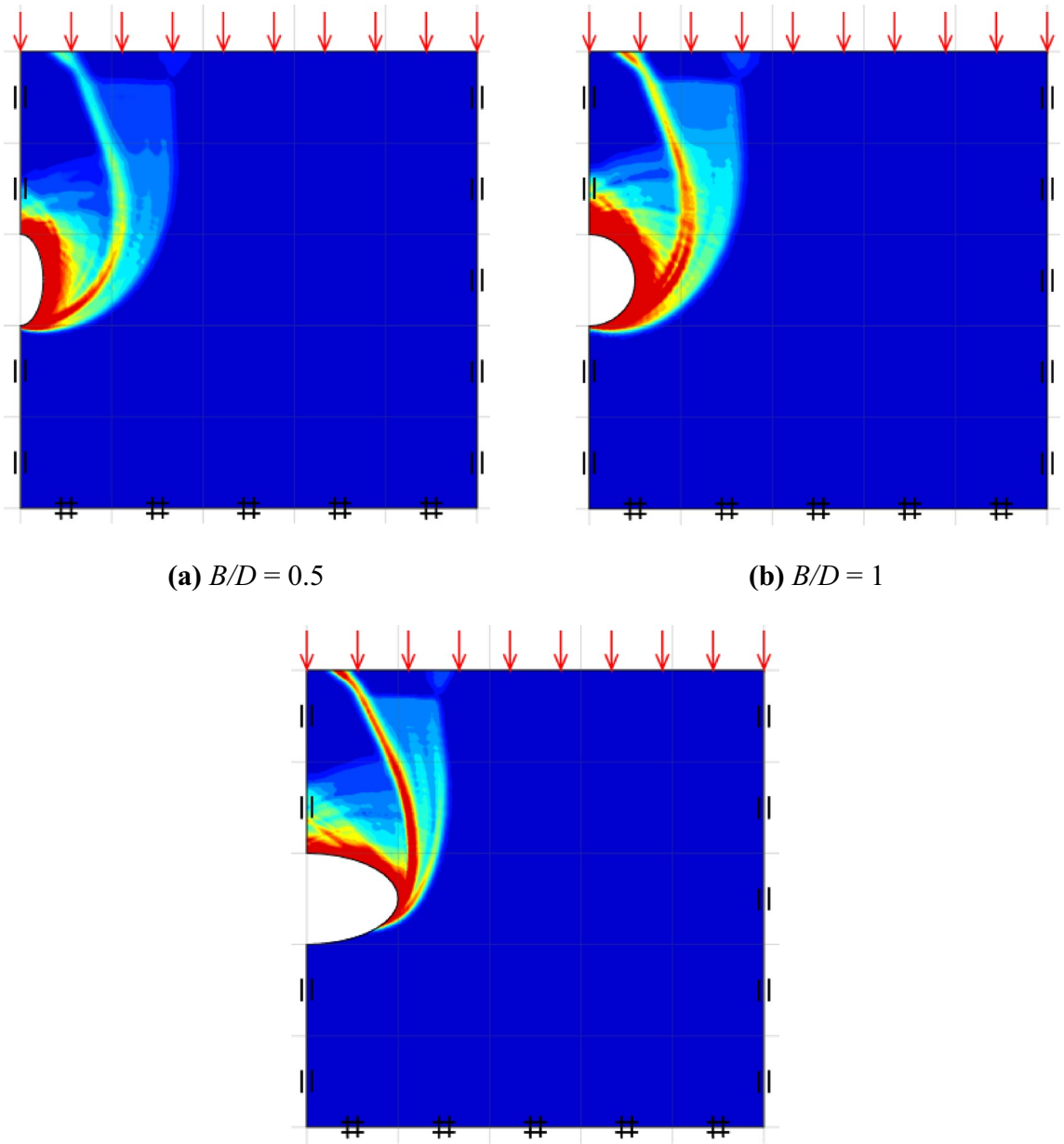

(a) $B/D = 0.5$ **(b)** $B/D = 1$

(c) $B/D = 2$

Fig. 10 Shear dissipations of unlined elliptical tunnel in rock mass ($C/D = 2$, $\sigma_{ci}/\gamma D = 1000$, GSI = 80 and $m_i = 20$)

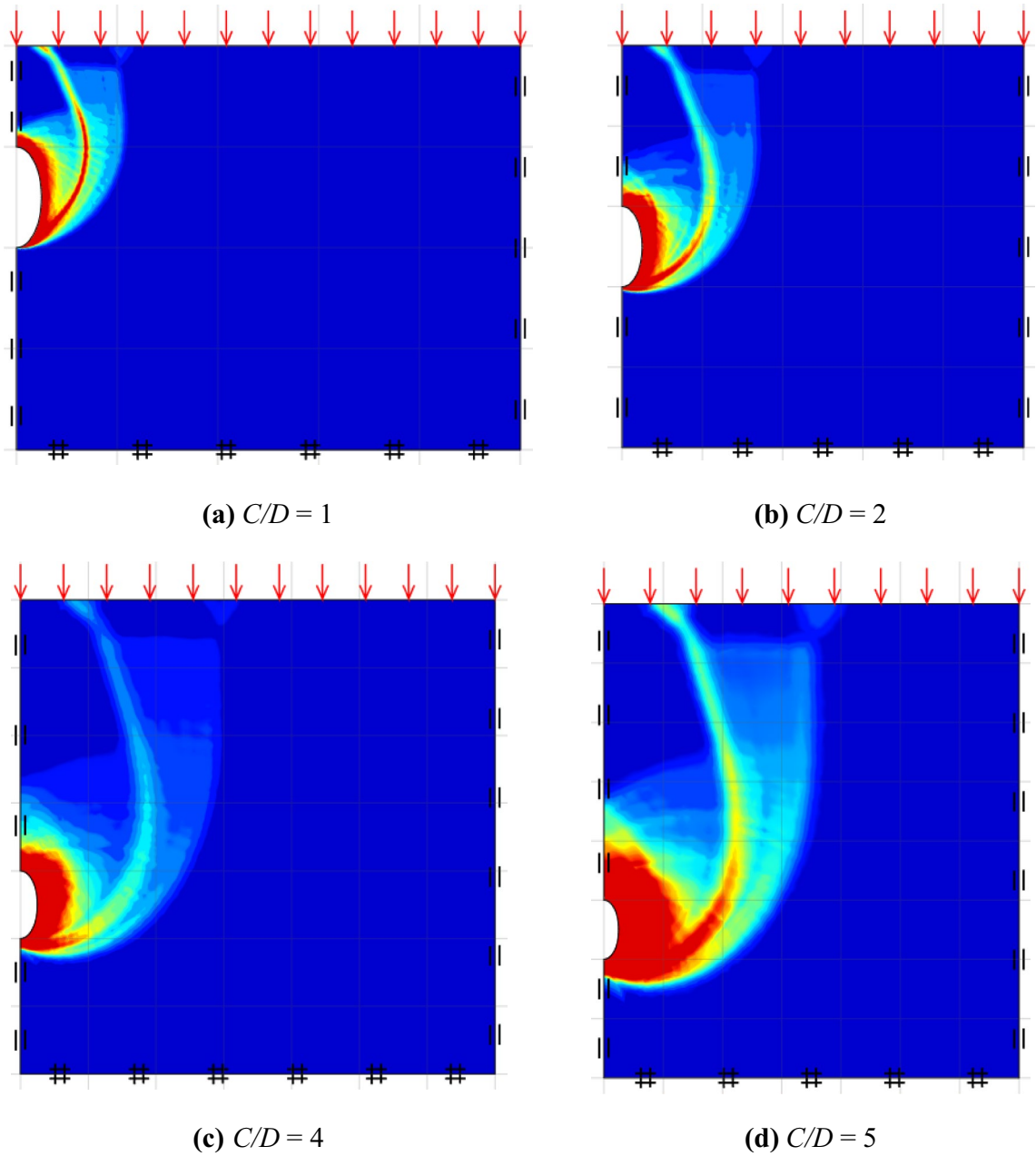

(a) $C/D = 1$ **(b)** $C/D = 2$

(c) $C/D = 4$ **(d)** $C/D = 5$

Fig. 11 Shear dissipations of unlined elliptical tunnel in rock mass with $B/D = 0.5$ ($\sigma_{ci}/\gamma D = 1000$, GSI = 80 and $m_i = 20$)

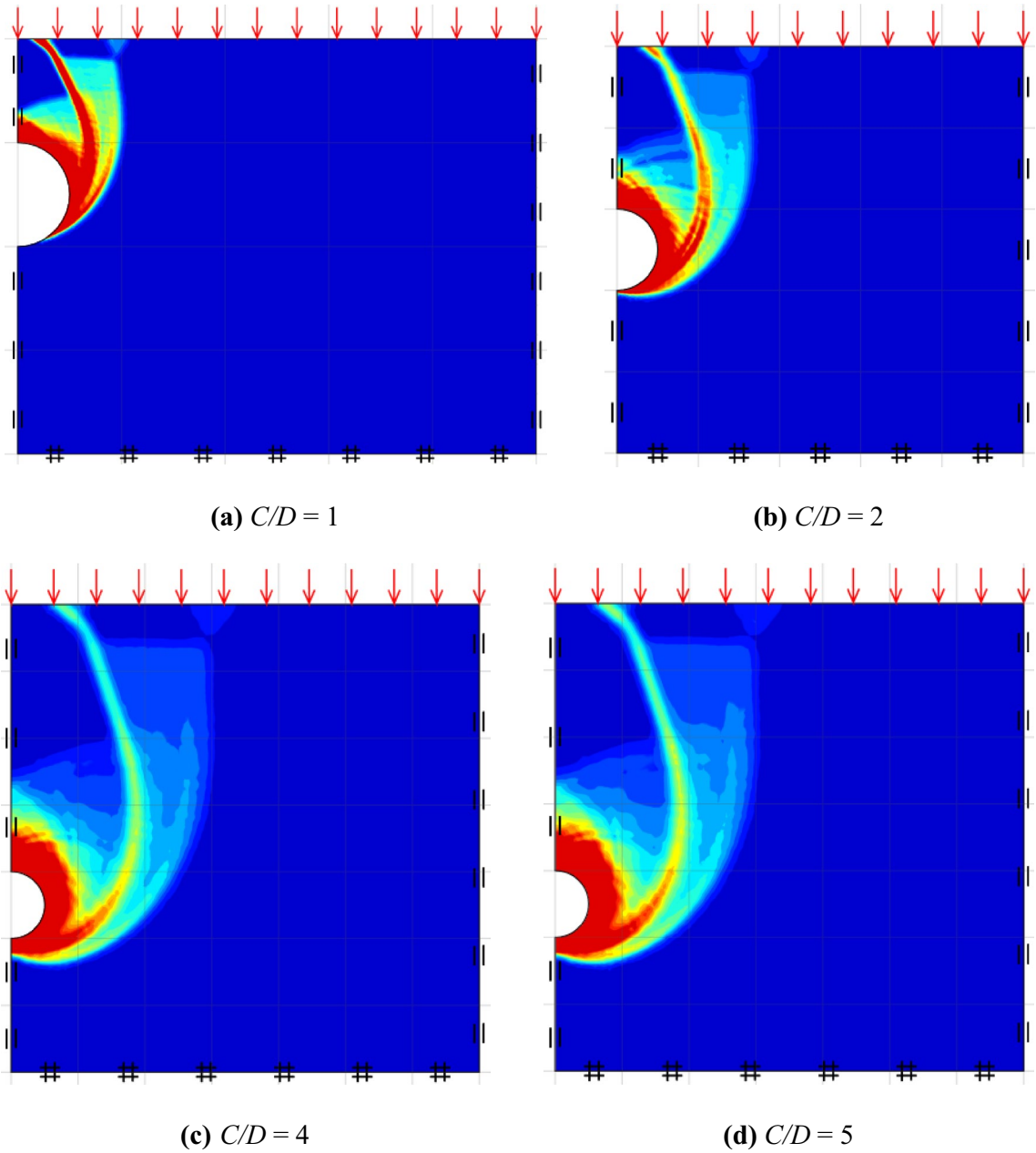

(a) $C/D = 1$ **(b)** $C/D = 2$

(c) $C/D = 4$ **(d)** $C/D = 5$

Fig. 12 Shear dissipations of unlined elliptical tunnel in rock mass with $B/D = 1$ ($\sigma_{ci}/\gamma D = 1000$, GSI = 80 and $m_i = 20$)

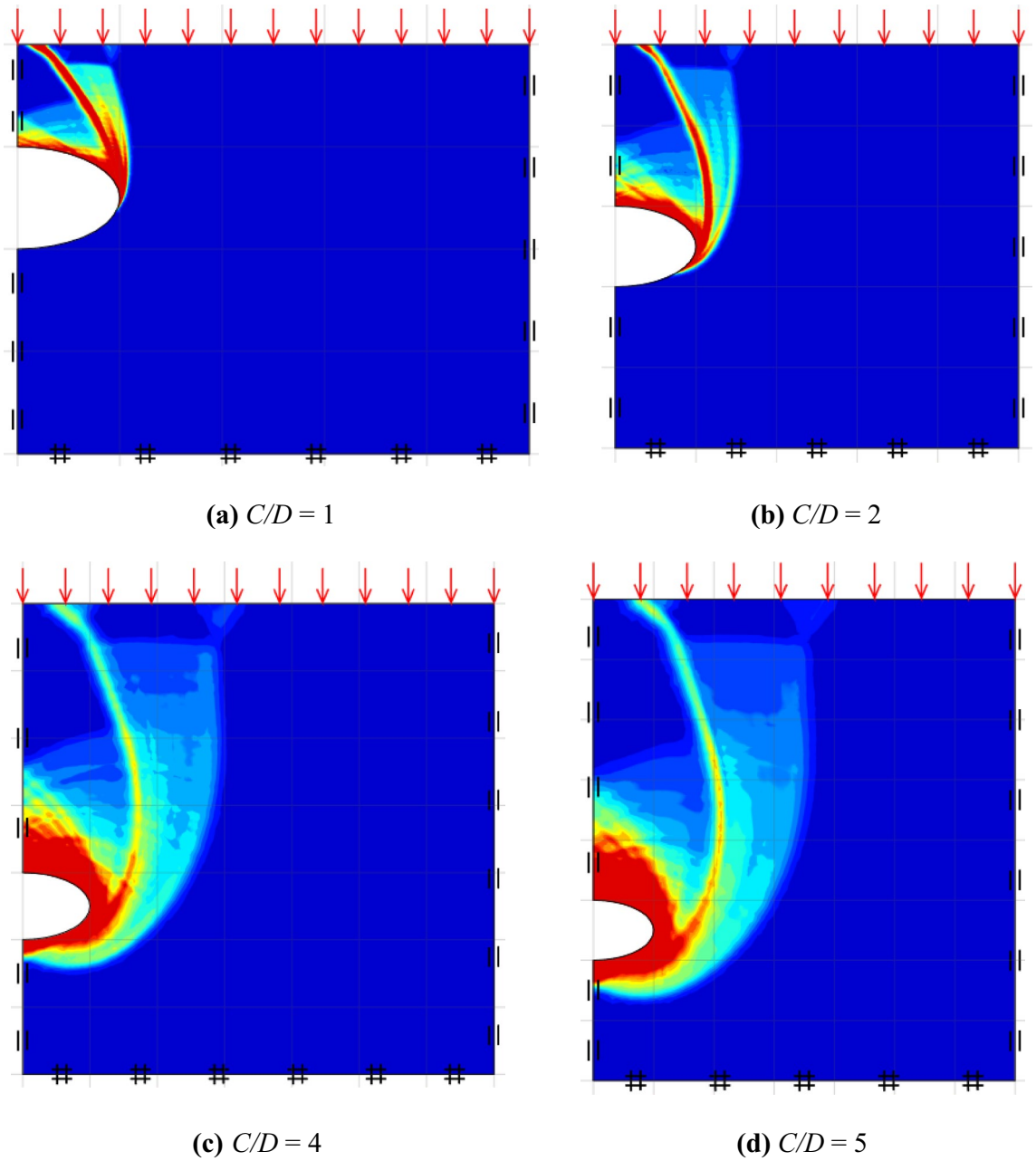

(a) $C/D = 1$ **(b)** $C/D = 2$

(c) $C/D = 4$ **(d)** $C/D = 5$

Fig. 13 Shear dissipations of unlined elliptical tunnel in rock mass with $B/D = 2$ ($\sigma_{ci}/\gamma D = 1000$, GSI = 80 and $m_i = 20$)

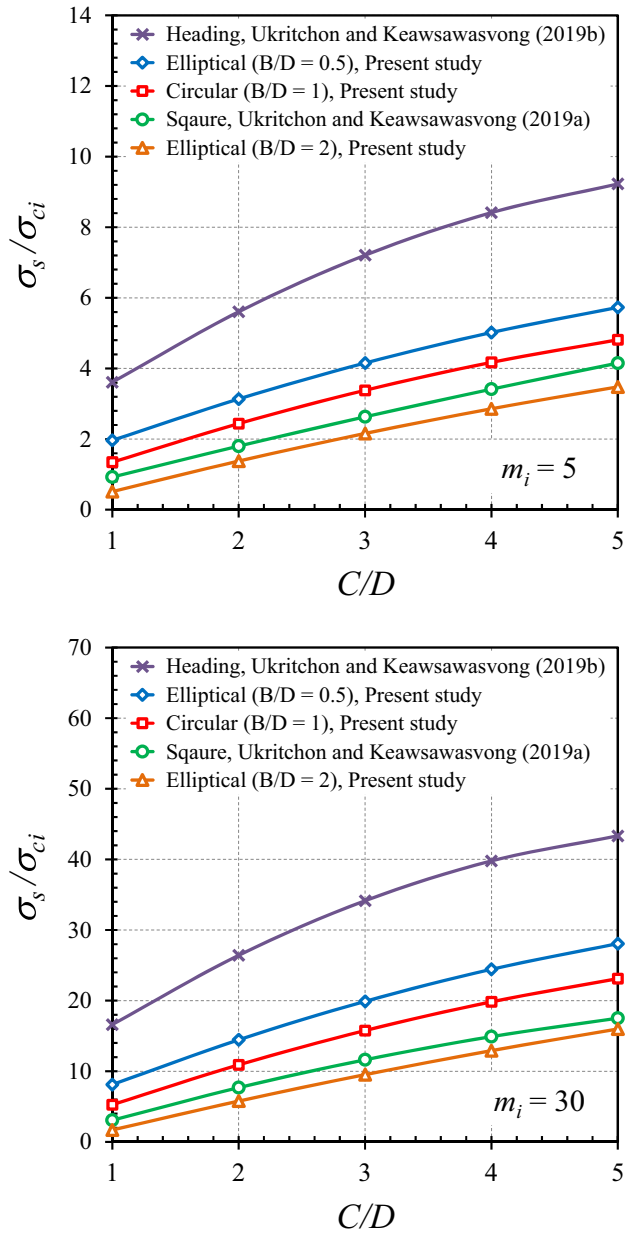

Fig. 14 Comparison of the stability factors σ_s/σ_{ci} for different shapes of tunnels ($\sigma_{ci}/\gamma D = 1000$ and GSI = 80)

Table 6 Optimal value of the constants for the design equations ($B/D = 0.5–2.0$)

Constants	B/D				
	0.50	0.75	1.00	1.33	2.00
a_1	-0.2247	-0.0888	-0.6843	-1.1022	-0.9402
a_2	-1.2896	-0.4498	-1.1308	-1.1149	-1.6978
b_1	0.02191	0.0233	0.0222	0.0217	0.0120
b_2	-0.03284	-0.0326	-0.0300	-0.0279	-0.0162
b_3	0.4917×10^{-2}	0.4872×10^{-2}	0.4404×10^{-2}	0.3981×10^{-2}	0.2068×10^{-2}
c_1	-0.1816×10^{-3}	-0.2130×10^{-3}	-0.2220×10^{-3}	-0.2379×10^{-3}	-0.1454×10^{-3}
c_2	0.4333×10^{-3}	0.4347×10^{-3}	0.4097×10^{-3}	0.3881×10^{-3}	0.2437×10^{-3}
c_3	-0.6180×10^{-4}	-0.6187×10^{-4}	-0.5693×10^{-4}	-0.5219×10^{-4}	-0.2814×10^{-4}
d_1	1.296×10^{-6}	1.1745×10^{-6}	1.0594×10^{-6}	9.2465×10^{-7}	7.0681×10^{-7}
e_1	0.1663	0.1213	0.0770	0.0244	-0.0433
e_2	-0.1854	-0.1607	-0.1367	-0.1092	-0.0682
f_1	-0.7268×10^{-2}	-0.5560×10^{-2}	-0.3839×10^{-2}	-0.1770×10^{-2}	0.1214×10^{-2}
f_2	0.0123	0.0109	0.9558×10^{-2}	0.7967×10^{-2}	0.5277×10^{-2}
f_3	-0.1867×10^{-3}	-0.1766×10^{-3}	-0.1590×10^{-3}	-0.1367×10^{-3}	-0.6488×10^{-4}
g_1	0.6635×10^{-4}	0.4659×10^{-4}	0.2800×10^{-4}	0.5795×10^{-5}	0.2281×10^{-4}
g_2	-0.1891×10^{-3}	-0.1683×10^{-3}	-0.1485×10^{-3}	-0.1254×10^{-3}	-0.8928×10^{-4}
R^2	99.98%	99.98%	99.98%	99.98%	99.98%

Author Contributions JS acquired methodology, software, conceptualization, and provided resources, writing—original draft. SK acquired methodology, software, conceptualization, and provided resources, writing—original draft. SS acquired software and contributed to the investigation and data curation.

Funding Open Access funding enabled and organized by CAUL and its Member Institutions.

Data Availability All data, models, and code that support the findings of this study are available from the corresponding author upon reasonable request.

Declarations

Conflict of Interest The authors declare that they have no conflicts of interest to this work.

References

Akagi H (2004) Geotechnical aspects of current underground construction in Japan. Soils Found 44(1):1–24. https://doi.org/10.3208/sandf.44.1

Amberg R (1983) Design and construction of the Furka base tunnel. Rock Mech Rock Eng 16:215–231

Bhattacharya P, Dutta P (2021) Estimation of lining pressure for stability of elliptical tunnel in cohesive-frictional soils. Proc Natl Acad Sci India Sect A Phys Sci. https://doi.org/10.1007/s40010-021-00742-z

Ciria H, Peraire J, Bonet J (2008) Mesh adaptive computation of upper and lower bounds in limit analysis. Int J Numer Meth Eng 75:899–944

Hochmuth W, Kritschke A, Weber J (1987) Subway construction in Munich, developments in tunneling with shotcrete support. Rock Mech Rock Eng 20:1–38

Hoek E, Brown ET (1980) Empirical strength criterion for rock masses. J Geotech Eng Div 106(9):1013–1035

Hoek E, Carranza-Torres C, Corkum B (2002) Hoek–Brown failure criterion—2002 edition. In: Proceedings of the North American rock mechanics society meeting in Toronto

Keawsawasvong S, Ukritchon B (2020) Design equation for stability of shallow unlined circular tunnels in Hoek–Brown rock masses. Bull Eng Geol Env 79:4167–4190

Liu J, Li P, Shi L, Fan J, Kou X, Huang D (2021) Spatial distribution model of the filling and diffusion pressure of synchronous grouting in a quasi-rectangular shield and its experimental verification. Undergr Space. https://doi.org/10.1016/j.undsp.2021.02.002

Miura K (2003) Design and construction of mountain tunnels in Japan. Tunn Undergr Space Technol 18:115–126

Miura K, Yagi H, Shiroma H, Takekuni K (2003) Study on design and construction method for the New Tomei–Meishin expressway tunnels. Tunn Undergr Space Technol 18:271–281

OptumCE (2020) OptumG2. Optum Computational Engineering, Copenhagen, Denmark. See https://optumce.com/

Sauer T (2014) Numerical analysis. Pearson Education Limited, London

Shiau J, Al-Asadi F (2018) Revisiting Broms and Bennermarks' original stability number for tunnel headings. Géotech Lett 8(4):310–314

Shiau J, Al-Asadi F (2020a) Two-dimensional tunnel heading stability factors Fc, Fs and Fγ'. Tunn Undergr Space Technol 97:103293

Shiau J, Al-Asadi F (2020b) Three-dimensional analysis of circular tunnel headings using Broms and Bennermarks' original stability number. Int J Geomech 20(7):0001734

Shiau J, Al-Asadi F (2020c) Three-dimensional heading stability of twin circular tunnels. Geotech Geol Eng 38(3):2973–2988

Shiau J, Al-Asadi F (2021) Revisiting circular tunnel stability using Broms and Bennermarks' original stability number. Int J Geomech 21(5):0001996

Shiau J, Smith C (2006) Numerical analysis of passive earth pressures with interfaces. In: III European conference on computational mechanics (ECCM 2006), Lisbon, Portugal

Shiau J, Pather S, Ayers R (2006a) Developing physical models for geotechnical teaching and research. In: Proc. 6th IC Physical Modelling in Geotechnics, pp 157–162

Shiau JS, Lyamin AV, Sloan SW (2006b) Application of pseudo-static limit analysis in geotechnical earthquake design. In: Schweiger HF (ed) Proc., 6th European Conf. on Numerical Methods in Geotechnical Engineering. Taylor & Francis, London, pp 249–255

Shiau J, Chudal B, Mahalingasivam K, Keawsawasvong S (2021) Pipeline burst-related ground stability in blowout condition. Transp Geotech 29:100587

Sloan SW (2013) Geotechnical stability analysis. Géotechnique 63(7):531–572

Ukritchon B, Keawsawasvong S (2017) Design equations for undrained stability of opening in underground walls. Tunn Undergr Space Technol 70:214–220

Ukritchon B, Keawsawasvong S (2019a) Stability of unlined square tunnels in Hoek–Brown rock masses based on lower bound analysis. Comput Geotech 105:249–264

Ukritchon B, Keawsawasvong S (2019b) Lower bound stability analysis of plane strain headings in Hoek–Brown rock masses. Tunn Undergr Space Technol 84:99–112

Wone M, Nasri V, Ryzhevskiy M (2003) Rock tunnelling challenges in Manhattan. In: 29th ITA World Tunnelling Congress, Amsterdam, vol 1, pp 145–151

Xiao Y, Zhao M, Zhang R, Zhao H, Wu G (2019) Stability of dual square tunnels in rock masses subjected to surcharge loading. Tunn Undergr Space Technol 92:103037

Xiao Y, Zhang R, Zhao M, Jiang J (2021) Stability of unlined rectangular tunnels in rock masses subjected to surcharge loading. Int J Geomech 21(1):04020233

Yang F, Zhang J, Yang JS, Zhao LH, Zheng XC (2015) Stability analysis of unlined elliptical tunnel using finite element upper-bound method with rigid translatory moving elements. Tunn Undergr Space Technol 50:13–22

Yang F, Sun XL, Zheng XC, Yang JS (2016) Stability analysis of a deep buried elliptical tunnel in cohesive–frictional soils with a nonassociated flow rule. Can Geotech J 54(6):736–741

Zhang J, Yang J, Yang F, Zhang X, Zheng X (2017) Upper-bound solution for stability number of elliptical tunnel in cohesionless soils. Int J Geomech 17(1):06016011

Zhang R, Xiao Y, Zhao M, Zhao H (2019) Stability of dual circular tunnels in a rock mass subjected to surcharge loading. Comput Geotech 108:257–268